Comparison of the effects of incineration, vacuum pyrolysis and dynamic pyrolysis on the composition of NMC-lithium battery cathode-material production scraps and separation of the current collector

(article starts on next page)

Full length article

Comparison of the effects of incineration, vacuum pyrolysis and dynamic pyrolysis on the composition of NMC-lithium battery cathode-material production scraps and separation of the current collector

Gabriele Lombardo[a,*], Burçak Ebin[a], Britt-Marie Steenari[a], Mahmood Alemrajabi[b], Ingrid Karlsson[b], Martina Petranikova[a]

[a] *Department of Chemistry and Chemical Engineering, Industrial Materials Recycling and Nuclear Chemistry, Chalmers University of Technology, SE-412 96, Gothenburg, Sweden*
[b] *Northvolt AB, Gamla Brogatan 26, 111 20 Stockholm*

ARTICLE INFO

ABSTRACT

The rising demand for lithium batteries is challenging battery producers to increase their production. This is causing an accumulation of production scrap which must be treated to allow re-utilization of cathode material in production. Several industrial lithium battery recycling processes use thermal pre-treatment in an oxidative or inert atmosphere, or in a vacuum, to separate the battery components and remove organic material. However, a comparison of the effects of incineration, dynamic pyrolysis (under a constant flow of inert gas), and pyrolysis under vacuum on the microstructure and composition of scrap cathode material has not been explored.

Scrap cathodes, with active material based on $Li(Ni_xMn_yCo_z)O_j$, were subjected to incineration, dynamic pyrolysis, and pyrolysis under vacuum at 450°, 550°, and 650°C for 30, 60, 90, and 150 min to determine the best approach to cathode material recovery. While the incineration did not cause any chemical transformation of cathode material, under pyrolysis conditions the organic components in the cathodes triggered carbothermic reduction of the active material, yielding Co_3O_4, NiO, Mn_3O_4, and Li_2CO_3 as products. In the gas by-products, formed from the decomposition of the organic material, CO, CO_2, and HF were determined. The decomposition especially of the binder in polyvinylidene fluoride (PVDF) facilitated the separation of the active material from the current collector by mechanical treatment. By subsequent ball milling, the best technique to recover cathode material is the incineration at a temperature higher than 550°C and below 650°C for at least 90 min, with > 95% of recovered active material.

1. Introduction

The Paris Agreement became effective on 4th November 2016 and was ratified by 187 parties. As its main goal, it limited the increase in global average temperatures to well below 2 °C above preindustrial levels. Furthermore, it called for efforts to limit the temperature increase to 1.5 °C. To this end, parties have to significantly reduce their anthropogenic emissions of greenhouse gasses (GHGs) (UNFCCC, 2015, Baldé et al., 2017). Of these emissions, the transport sector represents 23% and its electrification is therefore crucial to decreasing total GHGs. To match the goals set by the Agreement, the Norwegian government is applying policies to achieve sales targets of 100% zero-emissions vehicles by 2025. Denmark, Iceland, Ireland, Israel, the Netherlands, and Slovenia have announced that they will reach the same goal by 2030.

These are some of the reasons why the electric transport market is undergoing an important growth phase. Indeed, the data shows that the global stock of battery electric vehicles reached 5.1 million units in 2018; an increase of 63% in 2017, with the forecast suggesting that this trend is not going to change (International Energy Agency, 2018, Till Bunsen et al., 2019). All the major players in the car industry are increasing their investment to meet market demand. Carmakers such as Volkswagen, FCA, Ford, Hyundai-Kia, BMW, GM, and Renault-Nissan-Mitsubishi have announced between 10 and 40 new EV models each by the end of 2025. The Volvo Group has announced that 50% of its sales will be fully electric by 2025 (Till Bunsen et al., 2019).

* Corresponding author.
E-mail address: gablom@chalmers.se (G. Lombardo).

2. Background

Thanks to the increase in global electric car stock and the development of new technologies, the cost of manufacturing electric engines (the most expensive component of electric cars) is continuously reducing, increasing the competitiveness of electric engines with their traditional internal combustion counterparts. Nowadays, the major part of electric engine technology is based on Lithium-ion batteries (LiBs). These are also widely used in portable electronic devices and industrial applications due to their electrochemical performance, which includes high specific energy density. So, the increased demand for electric cars will lead to increased demand for LiBs and, thus, the raw materials necessary for their production (Hanisch et al., 2015).

Many of these raw materials are concentrated in two electrodes that compose the LiB cells: an anode (negative pole), generally composed of a copper layer covered by graphite, and a cathode (positive pole), generally composed of an Al layer coated with an active material (Xu et al., 2012). An organic binder made of polyvinylidene fluoride (PVDF) is normally used to increase adhesion between the active material and the Al layer (Li et al., 2013). The electrodes are then immersed in an electrolyte mixture of alkyl carbonates and Li salts and enclosed in a plastic casing (Chagnes, 2015, Diekmann et al., 2016). The performance of the battery cell is influenced by the chemistry of the cathode active material. The LiB type most used in the automotive field is the NMC-LiB, i.e. battery in which the cathode active material has the general composition $LiNi_{1-x-y}Mn_xCo_yO_2$, meaning they contain the metals manganese, nickel, cobalt, and lithium. Therefore, the growth in demand for LiBs determines the rise in requests for these raw metals. The increase in the electric vehicles market particularly influences the Li and Co markets. Indeed, in 2017, the demand for batteries accounted for 40% and 25% of demand for Li and Co respectively. If there is not still a lack in the supply of Mn, instead, Ni and Co, and soon also Li, are inserted in the list of the critical raw materials that have a high supply risk and are also crucial for the industrial base, growth, and competitiveness of Europe's economy (Azevedo et al., 2018).

One of the most promising methods to reduce the criticality of these raw materials seems to be recovering them from batteries through a recycling process (Gaines, 2014). Not just the spent end-of-life LiBs are involved in recycling processes but also a large quantity of LiB scraps generated by production processes (Zhang et al., 2016). Scraps have their own characteristics and so their recycling differs from the recycling of spent batteries. Scraps do not come into contact with the electrolyte and have not been subjected to charge/discharge cycles. This has as consequences that the recycling process is less dangerous but also more difficult because the active material is non-aged, which makes it harder to separate the active materials from the current collectors. The production processes, for their complexity, are generally affected by a significant scrap rate. Indeed, it is reported that the percentage of material inputs lost during the fabrication process is between 5% and 15% (Christian Hanisch et al., 2015; Schmuch et al., 2018). Given that materials represent almost 75% of the manufacturing costs of LiBs production, scraps need to be included in recycling strategies, to lower costs (Kwade et al., 2018).

The industrial recycling processes generally consist of a set of pre-processing methods, which do not alter the structure of the LIB cells, such as the sorting by battery type from mixed waste, generally based on their chemistry. The pre-processing methods are then followed by mechanical processes, hydrometallurgical processes, and pyrometallurgical processes. The mechanical process involves the use of techniques to dismantle the batteries classifying and concentrating materials basing on their physical and magnetically properties. These techniques do not alter the LiB cell chemistry and involve discharging and disassembling the batteries (Velázquez-Martínez et al., 2019). This is followed by chemical methods, such as hydrometallurgy, pyrometallurgy, or a mixture of both. (Christian Hanisch et al., 2015) Pyrometallurgy implies the use of elevated temperatures to trigger

redox reactions and burn the organic components and carbon, purifying the valuable metals. The products of this method are metallic alloys, from which it is possible to recover Co, Ni, and Cu, and a slag that contains Al, Mn, and Li. No consideration is given to the recovery of the electrolytes and the plastics and it is not possible to reclaim the metals in the slag without further hydrometallurgical treatment. However, pyrometallurgy remains a frequent method for the extraction of Co and Ni (Xiao et al., 2019, Korthauer, 2018). Furthermore, the battery organic components, such as and PVDF binder, and the graphite hinder the chemical reactions and reduce the efficiency of metal recovery (Granata et al., 2012). Thus, a thermal pre-treatment before the hydrometallurgical treatment is used to burn off the organic material. Furthermore, removing the organic binder during the thermal treatment enables the separation of the active material from the current collector by a mechanical treatment is facilitated. In this way, Cu and Al layers can be recovered before the hydrometallurgical treatment (Lv et al., 2018)(He et al., 2017). Thermal treatments can also trigger the carbothermic reduction reaction of the carbon present in the battery with the active material. The metal ions in the active material are reduced to lower oxidation and/or more soluble state. In this way, the addition of a reducing agent during the leaching can be avoided (Lombardo et al., 2019, Li et al., 2016). Other methods of removing the binder have been investigated, such as dissolution (Zeng and Li, 2014), ultra-sonic treatment (Li et al., 2009, Yao et al., 2018) and solvent extraction (Kim et al., 2004). PVDF binder can easily dissolve in certain organic solvents, such as N-methyl-2-pyrrolidone (NMP) and ionic liquids; it was observed that the use of ultrasonic treatment can help the process (Yao et al., 2015). However, it is difficult to scale up dissolution in the recycling process, due to the high cost of solvents and because it cannot remove all the impurities, so a further incineration treatment is needed to burn off the residues, such as carbon and PVDF (Zhang et al., 2018). Furthermore, the use of organic solvents like NMP carries important environmental restrictions. To decrease the environmental impact, thermal pre-treatment can be performed without the presence of oxygen.

2.1. State of the art of LiBs thermal treatment

The thermal pre-treatment can be performed in three alternative ways: incineration, pyrolysis under inert gas, or vacuum pyrolysis. In literature, incineration has been widely studied and the results show it to be highly efficient at removing organic components, which facilitates Co and Li leaching. Song et al., (2013) conducted double incineration to remove PVDF and recover scrap materials from NMC cathode material scraps. First, they sintered the scraps at 350–450 °C for two hours and the Al foil was separated from the scrap; then a hydrometallurgical method was used to recover $Li(Ni_{1/3}Co_{1/3}Mn_{1/3})O_2$ scrap materials and the sediment was heat-treated at 300–350 °C for one hour. Petráníková et al., (2011) incinerated the $LiCoO_2$ cathode material from spent portable batteries at 700 °C and observed an improvement in the Co and Li recovery rate due to $LiCoO_2$ reduction and carbon removal. Treating the same cathode material at 500 °C for five hours, Paulino et al., 2008) observed a complete removal of the carbon content. Compared to incineration, the amount of CO and CO_2 produced per time unit during pyrolysis is lower, so it is generally considered a greener process. Hu et al., (2017) conducted a roasting at 650 °C for three hours using Ar as the inert gas. They observed that the initial spent NMC cathode material was reduced into Ni, Co, and MnO, then leached out from the spent LiBs with H_2SO_4. Zhang et al., (2018) carried out pyrolysis at 500 °C for 30 min with a high-purity N_2 gas flow of 200 mL/min improving the separation of active material from the foils in the scrap. Lombardo et al., (2019) treated NMC-LiBs at 400–700 °C for 30–180 min with an N_2 gas flow of 340 mL/min. They showed that the increase in temperature and time of treatment enhances the carbothermic reduction as well as the removal of graphite and organic components. A valid alternative to using inert gas is the pyrolysis under vacuum

conditions. This was performed by Li et al. at 1000 °C for 30 min, obtaining a reduction of the $LiCoO_2$-LIB active material. (Li et al., 2016) Moreover, Xiao et al., (2017a) heated a mixture of $LiMn_2O_4$ and graphite in a vacuum furnace at 800 °C for 45 min under vacuum conditions and observed that the $LiMn_2O_4$ decomposed into Li_2CO_3 and MnO. Some studies (Schmuch et al., 2018; Song et al., 2019; Zheng et al., 2019) have shown that both calcination and pyrolysis can be used efficiently as a thermal treatment in recycling processes to regenerate the cathode material through structure reshaping.

One of the industrial recycling companies which applies a thermal pre-treatment in their processes is the German company, Accurec. It carries out the pyrometallurgical and hydrometallurgical recovery of Co Mn alloy and LiCl. The batteries are heated to a maximum temperature of 250 °C to evaporate the electrolyte solvent. Then Al, Cu, and organic binder are then separated by physical processes. (Vezzini, 2014) Umicore is another recycling company which uses a pyrometallurgical technology for battery recycling. It conducts thermal preheating of the battery cells to a maximum temperature of 300 °C (Christian Hanisch et al., 2015, Ekberg and Petranikova, 2015) .

2.2. Aim of this work

Almost all the published research has been carried out on spent batteries and so there is a lack of knowledge of the effects of thermal treatments on production scrap cathodes. However, this may also be interesting at an industrial level because, due to lack of carbon from the anode materials and electrolyte, thermal pre-treatment of production scrap cathodes could be designed with lower energy demands and more defined gas products, with a lower cost and environmental impact in comparison to the recycling of spent batteries.

In this work, NMC-LiB cathode production scraps were thermally treated at 450 °C, 550 °C and 650 °C for 30, 60, 90 and 180 min using three different methods: incineration with a constant flow of air, dynamic pyrolysis with a constant flow of inert gas, and pyrolysis under vacuum. A comparison of the effects on the microstructure of the $LiNi_{1-x-y}Mn_xCo_yO_2$ was performed. It was expected that the high temperature might trigger carbothermic reduction, with significant differences between the three methods.

Based on previous experience, it was concluded that the most efficient method for the recovery of active NMC material would be the combination of thermal pre-treatment and mechanical processing. By the utilization of the thermal pre-treatment, removal of the organic binder will be achieved. This is expected to facilitate the separation of the active material from the current collector in a mechanical treatment. To investigate this effect of the thermal treatment methods studied, a mechanical treatment with a ball mill was performed to observe how the level of separation varies with the time, temperature, and type of thermal treatment.

The decomposition of the binder and other organic components during the thermal treatment caused the formation of gas by-products that were characterized.

2.3. Thermodynamic consideration

During the thermal treatment, it is expected that the lithium-metal-oxide compounds are subjected to a carbothermic reduction, triggered by the carbon present in the PVDF. The partial pressure of the gasses involved in the described reactions, therefore mainly O_2 and CO, is the factor that can most modify the equilibrium of the chemical reactions, therefore the following reactions were written based on one molecule of these two gasses. Since the CO concentration inside the system is lower and less constant than the O_2 concentration, the reactions in which both these gasses are reagents are written based on one molecule of CO. Evidence at the support of the following reactions have been already presented in two previous works (Lombardo et al., 2019, Lombardo et al., 2020), in which thermodynamic calculations
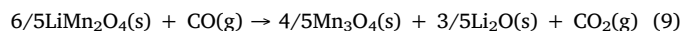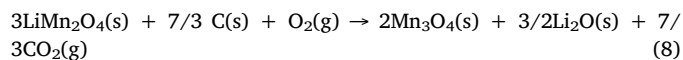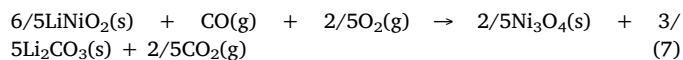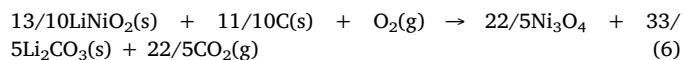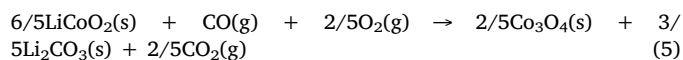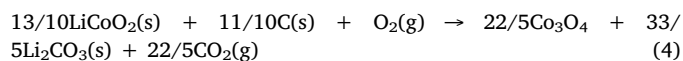
supported by XRD spectra about the carbothermic reactions that can take place during the thermal treatment of LIB cathodes have been already carried out.

2.4. Incineration

Under incineration conditions, the organic materials are consumed with the formation of CO2 and CO; reactions (1), (2), and (3).

$$C(s) + O_2(g) \rightarrow CO_2(g) \tag{1}$$

$$2C(s) + O_2(g) \rightarrow 2CO(g) \tag{2}$$

$$2CO(g) + O_2(g) \rightarrow 2CO_2(g) \tag{3}$$

If the C in the samples is abundant enough not to be completely consumed by the incineration but to also cause carbothermic reduction of the metal oxides and considering the cathode active material as a homogeneous mix of $LiCoO_2$, $LiMn_2O_4$, and $LiNiO_2$, C and CO are involved in the following reduction reactions:
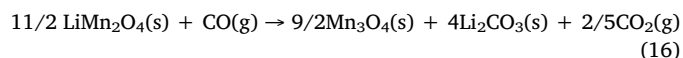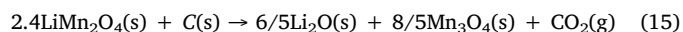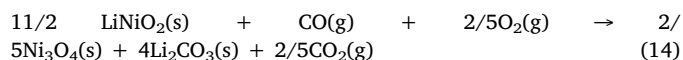
$$13/10 LiCoO_2(s) + 11/10 C(s) + O_2(g) \rightarrow 22/5 Co_3O_4 + 33/5 Li_2CO_3(s) + 22/5 CO_2(g) \tag{4}$$

$$6/5 LiCoO_2(s) + CO(g) + 2/5 O_2(g) \rightarrow 2/5 Co_3O_4(s) + 3/5 Li_2CO_3(s) + 2/5 CO_2(g) \tag{5}$$

$$13/10 LiNiO_2(s) + 11/10 C(s) + O_2(g) \rightarrow 22/5 Ni_3O_4 + 33/5 Li_2CO_3(s) + 22/5 CO_2(g) \tag{6}$$

$$6/5 LiNiO_2(s) + CO(g) + 2/5 O_2(g) \rightarrow 2/5 Ni_3O_4(s) + 3/5 Li_2CO_3(s) + 2/5 CO_2(g) \tag{7}$$

$$3 LiMn_2O_4(s) + 7/3\ C(s) + O_2(g) \rightarrow 2 Mn_3O_4(s) + 3/2 Li_2O(s) + 7/3 CO_2(g) \tag{8}$$

$$6/5 LiMn_2O_4(s) + CO(g) \rightarrow 4/5 Mn_3O_4(s) + 3/5 Li_2O(s) + CO_2(g) \tag{9}$$

$$CO_2(g) + 2 Li_2O(s) \rightarrow Li_2CO_3(s) \tag{10}$$
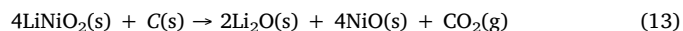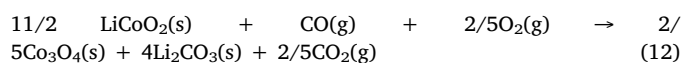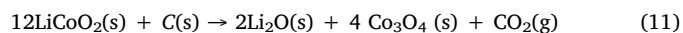
Some of the Co^{III} in the $LiCoO_2$ is reduced by C and CO with $Co^{II}(Co^{III})_2O_4$ as product, as described in reactions (4) and (5). Ni has a similar reaction pattern and its reduced forms are $Ni^{II}(Ni^{III})_2O_4$.

$LiMn_2O_4(s)$ is reduced to $Mn^{II}(Mn^{III})_2O_4$, as shown in reactions (8), and (9). Li tends to maintain its oxidation state and form stable Li_2O. The carbon is oxidized to CO and CO_2. The reaction between CO_2 and Li_2O produces Li_2CO_3, as described by Eq. (10).

2.5. Pyrolysis

Under pyrolysis conditions, both C and CO are involved in the following reduction reactions:

$$12 LiCoO_2(s) + C(s) \rightarrow 2 Li_2O(s) + 4\ Co_3O_4\ (s) + CO_2(g) \tag{11}$$

$$11/2\quad LiCoO_2(s)\quad +\quad CO(g)\quad +\quad 2/5 O_2(g)\quad \rightarrow\quad 2/5 Co_3O_4(s) + 4 Li_2CO_3(s) + 2/5 CO_2(g) \tag{12}$$

$$4 LiNiO_2(s) + C(s) \rightarrow 2 Li_2O(s) + 4 NiO(s) + CO_2(g) \tag{13}$$

$$11/2\quad LiNiO_2(s)\quad +\quad CO(g)\quad +\quad 2/5 O_2(g)\quad \rightarrow\quad 2/5 Ni_3O_4(s) + 4 Li_2CO_3(s) + 2/5 CO_2(g) \tag{14}$$

$$2.4 LiMn_2O_4(s) + C(s) \rightarrow 6/5 Li_2O(s) + 8/5 Mn_3O_4(s) + CO_2(g) \tag{15}$$

$$11/2\ LiMn_2O_4(s) + CO(g) \rightarrow 9/2 Mn_3O_4(s) + 4 Li_2CO_3(s) + 2/5 CO_2(g) \tag{16}$$

$LiCoO_2$ is reduced by C and CO to form $Co^{II}(Co^{III})_2O_4$, as described by reaction (11). The carbothermic reduction of Ni^{III} can give $Ni^{II}O$ as the main product, as described by reaction (13). Mn with oxidation states III and IV in $LiMn_2O_4$ is reduced to $Mn^{II}(Mn^{III})_3O_4$. Li is also converted to Li_2CO_3 in this condition.

2.6. PVDF

Among the organic components, PVDF and its decomposition process have a central role in the separation of the active material from the aluminum layer. The majority of the PVDF chains have a regular structure of alternating CH_2 and CF_2 groups (Dargaville et al., n.d.), with a fluorine content of 60% by weight (Inderherbergh, 1991). PVDF is a crystalline polymer of quite high thermal stability and its thermal decomposition is heavily influenced by the presence of O_2 (Hirschler, 1982). Indeed, it has been observed through thermal gravimetric analysis that the degradation of PVDF begins at around 450 °C in air and with a weight loss of over 80% before the temperature at which the decomposition in N_2 begins, ~ 480 °C (Nguyen, 1985). It has been concluded that O_2 reduces the activation energy of the thermal degradation. This involves the release of gas containing HF and the monomer vinylidene fluoride (VDF). The release of HF determines the formation of double bonds in the polymer chain and even possible cross-linking (Zulfiqar et al., 1994). There is as well the formation of the dimer of VDF and bigger aliphatic and cyclic molecules that remain in the liquid fraction (Choi and Kim, 2012).

3. Materials and methods

3.1. Samples preparation

The starting material was composed of a LiB ribbon-shaped cathode composed consisting of an Al layer, 19.4 cm wide and 300 cm long (Fig. 1). It is the scrap of a LiB cathode production chain. To prepare each sample, an area of 100 cm^2 covered by the active material was cut from the layer, weighed, and divided into pieces of approximately 5 cm^2. Samples of weight 1.95 ± 0.3 g were prepared.

3.2. Thermal treatment

The samples were thermally treated at 450, 550, or 650 °C for 30, 60, 90, or 150 min. The thermal treatment was performed inside a tubular furnace (Nabertherm GmbH Universal Tube Furnace RT 50–250/11) and thermally insulated. Each sample was placed in an alumina sample holder and inserted into a high-purity 65 cm alumina tube (Al_2O_3, 99.7%, Degussit AL23, Aliaxis). Stainless steel, custom-made connectors were added to both ends of the tube. Only when the furnaced reached the selected temperature, the alumina tube was then inserted in the tubular furnace. A constant flow of approximately 340 ml/min of 99.9% pure nitrogen (for the dynamic pyrolysis) or air (for the incineration) was pumped through the tube, with a flow meter used to regulate the gas flow at the system inlet. The exhaust gas was bubbled through three plastic cylinders filled with 100 ml of MilliQ water (ultrapure water with a resistivity of 18.2 MΩ.cm (at 25 °C) and a TOC value below 5 ppb). For the vacuum pyrolysis, a vacuum of − 0.75 bar was applied to the system with a Millipore vacuum pump.

Firstly a constant flow of N_2 was injected in the furnace to remove the partial pressure of oxygen before the vacuum is formed. Once the furnace was up to temperature and the vacuum condition was achieved, the samples were inserted in the furnace and each end of the alumina tube was closed with a valve, to keep the pressure in the tube constant. The vacuum pump was then turned off.

3.3. Experiments were carried out in triplicate

3.3.1. Mechanical treatment

A Fritsch Planetary Mill Pulverisette 7 was used. The machine consists of a rotation plate with two symmetrical holders. Each holder hosts a sample holder that contains quartz balls with a diameter of 1 cm. After the thermal treatment, the cathode was inserted in the ball mill sample holders for 15 mins at 1000 rpm. The same treatment was applied to untreated samples, to compare the efficiency of the black mass removal and contribution of the thermal treatment. The samples, the internal surface of the sample holders, and the quartz balls were washed with MilliQ water in order to recover all the cathode material detached from the Al foil. The removed cathode active material was then left in the air to dry and weighed.

3.3.2. Experiments were carried out in triplicate

3.3.2.1. X-ray powder diffraction qualitative analysis of crystalline compounds – XRD. The XRD analyses were carried out using a Siemens D5000 X-ray diffractometer. An accelerator voltage of 40 kV and a current of 40 mA were used. The X-ray wavelength used corresponds to the characteristic Cu K-radiation with a 2Θ range scan from 10° to 80° Furthermore, sample rotation at15 rpm was used to avoid any preferential orientation of the crystals causing incorrect peak heights. The diffraction data obtained was evaluated by comparison with standard data for known compounds in the JCPDS database("[JCP 13] JCPDS – International Center for Diffraction Data, PDF – 4+ (2013), 12 Campus Blvd., Newton Square, PA 19,073 – 3273 U.S.A.," n.d.).

3.3.2.2. Determination of metal concentrations in solid samples by ICP-OES analysis. The dissolution of the electrode materials was carried out using aqua regia (Merck Millipore Nitric acid 65% - EMD Millipore Hydrochloric acid 37%) at approximately 80 °C using magnetic stirring. The resulting solutions were filtered. The liquid fraction was diluted 100 times by using 0.5 M HNO_3 (Merck Millipore Nitric acid 65%) and an iCAP™ 6000 Series ICP-OES was used to determine the metal concentrations in the solutions.

3.3.2.3. Fourier-transform infrared spectroscopy (FTIR) analysis of gas produced during thermal treatment. A Perkin Elmer Spectrum Two FT-IR Spectrometer - standard detector was used, equipped with an $LiTaO_3$ detector, which has a range between 15,700 – 370 cm-1. The sample holder was a cell equipped with gas-tight taps, the ends of which are

Fig. 1. Cathode scrap material.

closed with flat-glass KBr walls.

3.3.2.4. Analysis of carbon content based on combustion in O_2. A LECO CS744 instrument was used to determine the carbon content of the samples before and after thermal treatment.

3.3.2.5. Ion chromatography. The MilliQ water, used to wash the gas exiting from the furnace, was analyzed using a Dionex DX100 Ion chromatograph, to measure the concentration of anions. The column used was a Dionex IonPacTM AS4A-SC RFICTM 4 × 250 mm Analytical. The eluent was a solution of 1.7 mM $NaHCO_3$ and 1.8 mM Na_2CO_3.

3.3.2.6. Scanning electron microscope (SEM). The morphology of the samples was investigated using a FEI Quanta 200 environmental SEM equipped with an Oxford Inca energy dispersive X-ray detector (EDX). Imaging was done with accelerating voltages at 20 kV.

4. Results and discussion

4.1. Characterization of the cathode material

The weight of the active material and PVDF that covered 100 cm^2 of Al layer is approximately 1.60 ± 0.02 g and represented the main component of the cell, ~83%w, followed by the Al foil with 0.33 ± 0.01 g, ~17%w.

The concentrations of the metals in the cathode material, obtained through ICP-OES analysis, are given in Table 1.

The main component of the active material is Ni with seven times higher concentration than that of Co and almost fourteen times higher than that of Mn. The remaining almost 10 wt% is due to the presence of the C and the PVDF.

4.2. X-ray analyses

X-ray analyses were conducted to determine how the thermal treatment influences the microstructure and composition of the samples. All the detected peaks in the XRD spectrum of the untreated cathode active material (shown in Fig. 2) are due to the presence of the $Li(Ni_xMn_yCo_z)O_2$. It is not possible to observe any significant difference when comparing this one with the spectra of incinerated cathode active material. This indicates that, under incineration conditions, thermal treatment does not change the composition or microstructure of the active material. The O_2 reacts with the entire quantity of C in the samples, as described in reactions (1), (2) and (3), with CO and CO_2 as products brought out of the system by the constant airflow. The spectra of the cathode active materials subjected to vacuum pyrolysis at 450 °C and 550 °C showed similar results (Fig. 3a). Only after a reaction carried out at 650 °C for 90 min it was possible to detect the signals of Li_2CO_3, Mn_3O_4, Co_3O_4, and NiO (Fig. 3b).

As anticipated from the reactions (11)-(16). Co, Mn, and Ni are obtained at a lower oxidation state after 30 min of treatment at 650 °C. Co_3O_4, Mn_3O_4, and Li_2CO_3 are the main products. It was expected the presence of Ni_3O_4, but it further decomposes according to reaction 17.

$$Ni_3O_4 + CO \rightarrow 3NiO + CO_2 \qquad (17)$$

The same carbothermic reduction products were observed as early as 450 °C in the samples pyrolyzed under inert gas, Fig. 4. It may be concluded that the constant flow of nitrogen in the system during

Table 1
Metal composition of the battery [wt%].

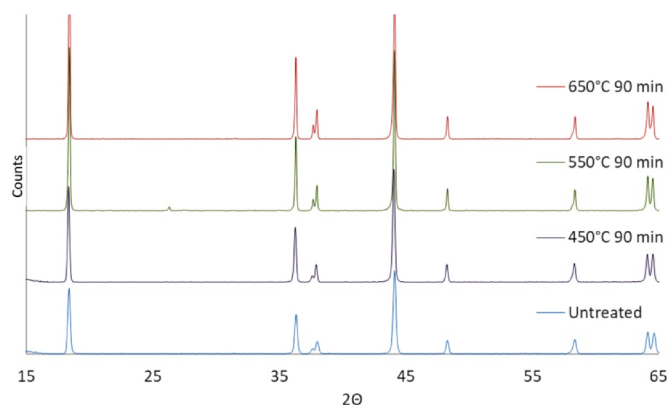| Mn	Ni	Co	Li	Al
3.3 ± 0.1	51.0 ± 1.3	7.0 ± 0.2	7.0 ± 0.2	22.2 ± 0.7

Fig. 2. Comparison between the XRD spectra of an untreated sample and the spectra of samples incinerated 90 min at 450 °C, 550 °C, or 650 °C.
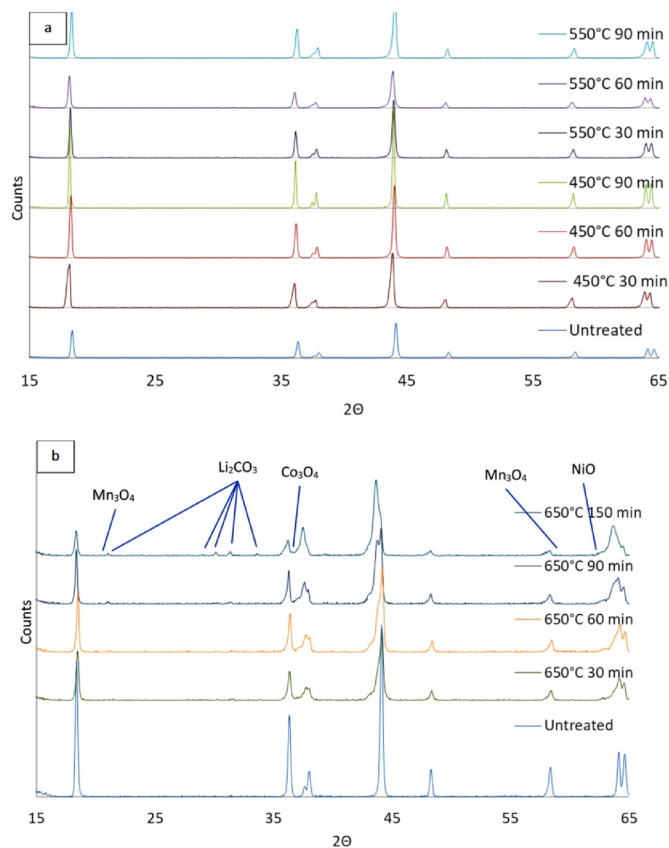

Fig. 3. (a, b: Comparison between the XRD spectra of an untreated sample and the spectra of samples thermal treated in vacuum condition 30, 60, 90, or 150 min at 450 °C, 550 °C, or 650 °C.

pyrolysis promotes the carbothermic reaction, bringing the CO_2 out of the system that was produced during the reduction.

The peaks at 18° and 44° are typical of the $Li(Ni_xMn_yCo_z)O_2$ compounds. Their presence in the spectra even after 150 min of treatment at all temperatures indicates that the conditions of treatment are not enough severe or the quantity of carbon is not enough to give a complete reduction of the metal oxides. Indeed, Li et al., (2016) have proved that carrying out a pyrolysis at higher temperature, 1000 °C for 30 min, and adding graphite until to obtain a molar ration $LiCoO_2$/ graphite of at least 4/3, it is possible to push the reduction of $LiCoO_2$ to form metallic Co and Li_2CO_3. Also, Xiao et al., (2017b), performing vacuum pyrolysis on NMC-LiB, observe that it is possible to reduce $LiCoO_2$ and $LiMn_2O_4$ to metallic Co and MnO, performing a thermal treatment at a
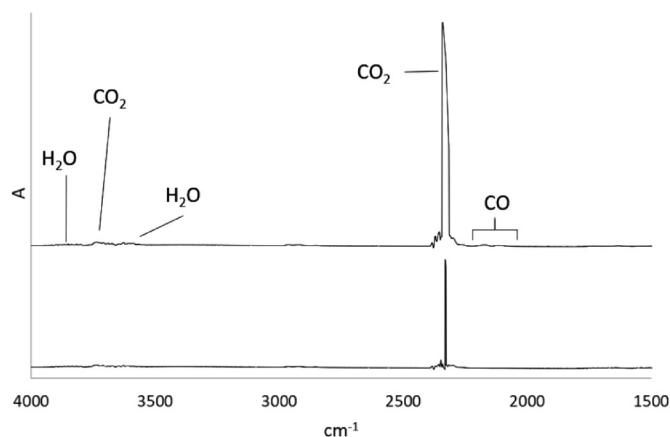
Fig. 5. Comparison of IR absorbance spectra for samples treated for 10 min at 550°C, for pyrolysis and incineration respectively.

temperature slightly higher, 700 °C, and adding the graphite remove from the LiB anodes.

4.3. Off-gas analysis

The formation of CO_2 was detected when analyzing the off-gas from the furnace (Fig. 5) during the incineration and dynamic pyrolysis.

Comparing with the pyrolysis, the FTIR spectra of the gas produced during incineration have wider and higher peaks for CO_2. Furthermore, the presence of CO was detected; the signal for this is absent in the gas produced during pyrolysis. During the thermal treatment, the quantity of C present in the samples decreases because it reacts with the cathode active material and with oxygen producing CO and CO_2. A carbon analyzer was used to quantify the residual carbon in the samples. In the untreated samples, the carbon content was measured equal to 8.01 ± 0.33 w%. The content in the incinerated and pyrolyzed after treatment for 150 min at 550 °C samples was respectively 2.03 ± 0.20 w% and 5.77 ± 0.30 w%. The difference between the carbon content in the untreated and treated samples gives an indication of the quantity of CO and CO_2 during the treatment, ~6 w% and ~2 w% respectively.

The signal for H_2O at high frequency probably covers the HF signal, the presence of which was expected since due to binder degradation taking place. The formation of HF during the treatment was confirmed by analyzing the MQ water used for washing the off-gas by ion chromatography for fluoride ions. The presence of fluoride, one of the decomposition products of the PVDF, was detected for samples after treatment for 150 min at 550 °C in a concentration of 217.53 ± 2.01 μM/g in incineration conditions and 213.23 ± 7.01 μM/g in pyrolysis under inert gas conditions. By contrast, one of the advantages of vacuum pyrolysis is that there are no gas emissions from the system during treatment. At the end of the process, the pressure is neutralized and the evacuated produced gas can be easily washed. This gives this process a significative reduction in environmental impact and costs of toxic gas abatement. The gas produced remains inside the system and the pressure is increased from -0.75 to ~ -0.6 bar. Both (Choi and Kim, 2012 and Diaz et al., 2019) have shown that the gas by-products should contain aromatic fluoride and fluorinated dioxins. In general, incineration produces more off-gas but the toxicity of off-gas is reduced compared to pyrolysis. Even though no evidence for the formation of these compounds was found in the present study, their possible existence is an important issue and we will study it further in our continued work.
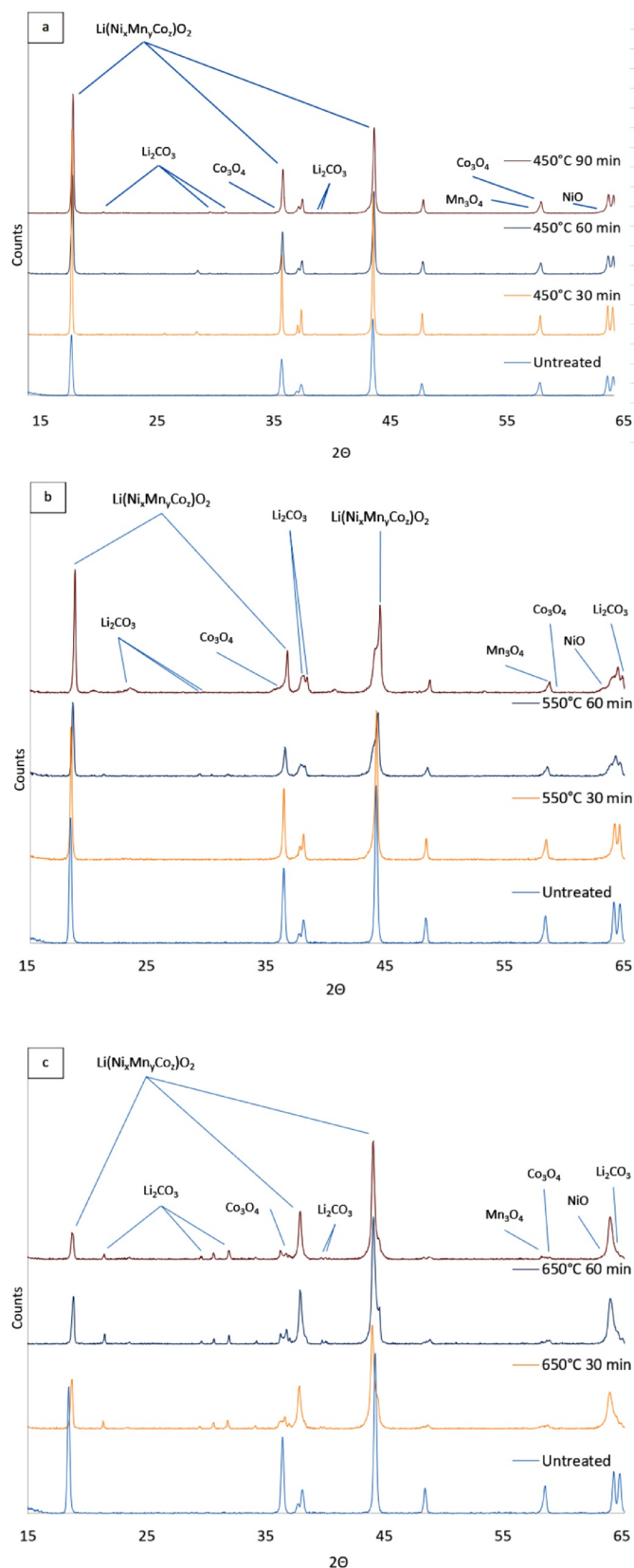

Fig. 4. (a, b,c: Comparison between the XRD spectra of an untreated sample and the spectra of samples pyrolysed for 30, 60, or 90 min at 450 °C, 550 °C, or 650 °C.
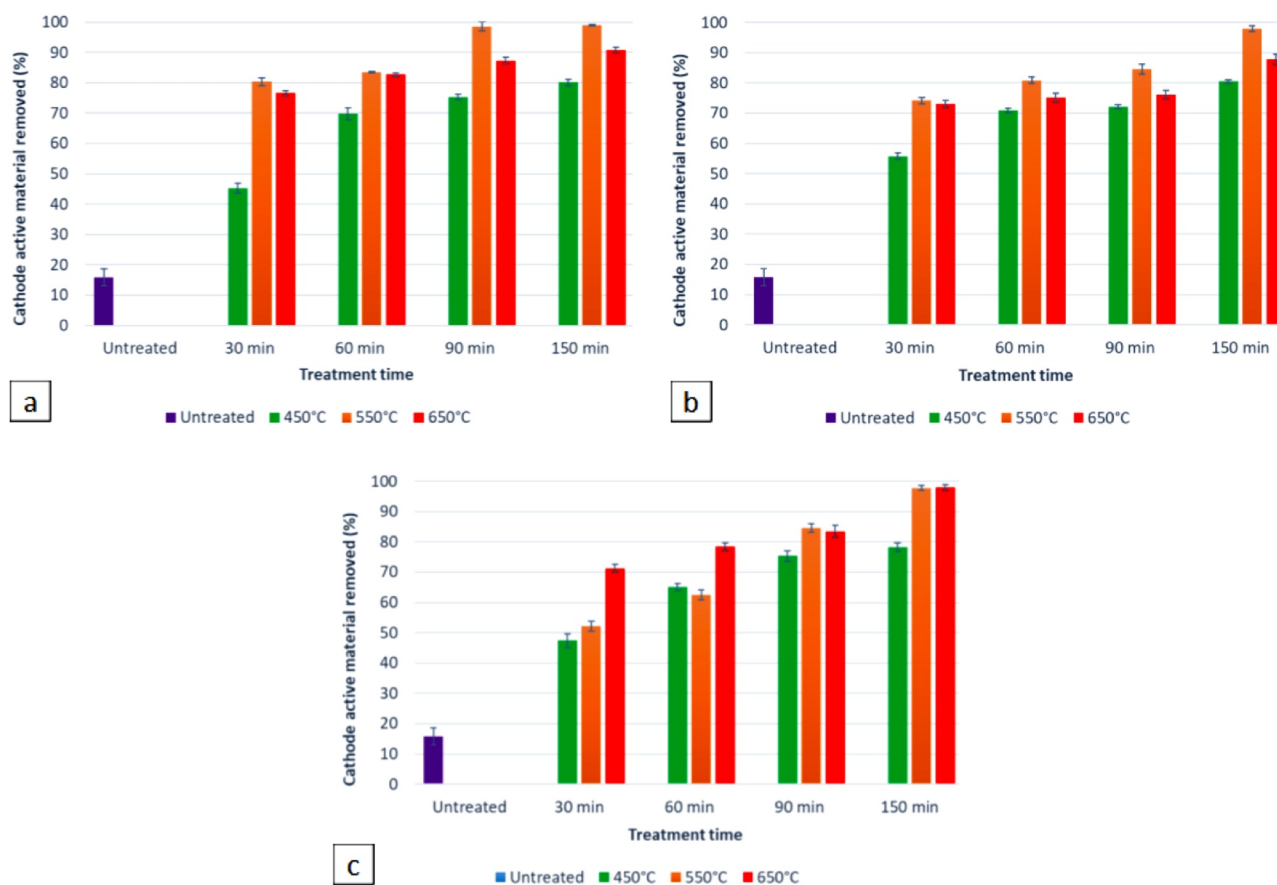
Fig. 6. Comparison between cathode active material recovered after 15 min of milling from the untreated samples with the quantity recovered from samples a) incinerated, b) pyrolyzed under inert gas and c) subjected to vacuum pyrolysis (c). (For interpretation of the references to colour in this figure legend, the reader is referred to the web version of this article.)

4.4. Mechanical separation of black mass from the Al layer without and after the thermal treatment

After the thermal treatment, the effectivity of active material removal from the foils was studied through a mechanical treatment performed in a ball mill. In the milling of the samples that had not been thermally treated, only 15.8% of the cathode material could be separated. Instead, it was observed that higher temperature used in the thermal treatment increases the separation efficiency in the milling.

4.5. Incineration

Increasing the time and temperature of treatment positively affected the quantity of active material removed from the Al layer. The plot in Fig. 6a shows that after 60 min of incineration, the quantity of active material removed increases from 69% for treatment at 450°C to 83% at 550°C. No significant difference in the amount of active material removed was noticed for temperatures between 550° C and 650°C (Table 2). After 90 min at 550°C, an almost complete separation of active material is possible, with 98.6% of material removed. A comparison with the untreated samples shows the incineration efficiency; after 15 min in the mill, the quantity of material removed from the treated cathodes is seven times higher than the quantity obtained from the untreated ones. For more details, refer to Table 2.

4.6. Dynamic pyrolysis and vacuum pyrolysis

The milling after the pyrolysis shows a lower efficiency in the separation of active material from the Al layer, since complete separation is possible only after 150 min of heat treatment. After thermal treatment under inert gas, the quantity of active material removed through mechanical treatment rises from ~56%, after 30 min of treatment at 450°C, to its maximum at 84% after pyrolysis at 550°C after 90 min (Fig. 6b-Table 2). Instead, after vacuum pyrolysis, the active material removed by milling increases from ~47% for 30 min treatment at 450°C to 84% at 550–650°C after 90 min (Fig. 6c-Table 2).

After both incineration and dynamic pyrolysis, the quantity of active material removed through milling is significantly higher for the samples treated for 90 min at 550°C than for those treated at 650°C. The main reason is the partial melting of the Al foil (660.3 °C). At 650 °C, Al melt covered the cathode material and inhibited PVDF removal.

The quantity of active material through removed milling is greater for the samples treated for a longer time and at higher temperature. However, there are differences between the two kinds of pyrolysis conducted. Indeed, after dynamic pyrolysis, the quantity of materials removed through milling is already over 50% of the total after thermal treatment at 400 °C for 30 min and grows rapidly, reaching over 80% of material removed after treatment at 550 °C for 60 min. By contrast, to reach the same value of material removed by vacuum pyrolysis, it is necessary to treat the samples at a temperature above 550 °C for at least 90 min. This is due to the presence of the N_2 flow which constantly removes the PVDF decomposition products from the furnace, thus promoting its decomposition.

4.7. Morphology and particle size of active material

The study of the effects of the thermal treatment on the morphology and particle size of cathode active material separated from the current collector is important for the subsequent leaching and regeneration for lithium ion batteries. Observing Fig. 7, it is possible to compare the

Table 2
Recovered cathode active material after 15 min of milling from the untreated and thermal treated cathode samples.

		Average cathode active material recovered after milling (%)			
	Untreated	15.80 ± 0.20			
	Treatment time	30 min	60 min	90 min	150 min
Incineration	450 °C	45.21 ± 1.72	69.80 ± 1.31	75,29 ± 0.90	80.12 ± 1.00
	550 °C	80.39 ± 2.01	83.41 ± 0.22	98,59 ± 0.52	99.01 ± 0.53
	650 °C	76.56 ± 1.01	82.68 ± 1.48	87,29 ± 1.02	90.7 ± 0.91
Dynamic pyrolysis	450 °C	55.74 ± 1.04	70.90 ± 1.06	72.16 ± 0.17	80.45 ± 0.54
	550 °C	74.10 ± 0.84	80.83 ± 2.02	84.58 ± 1.34	97.90 ± 1.03
	650 °C	72.99 ± 0.72	75.15 ± 1.22	76.06 ± 1.45	87.87 ± 1.60
Vacuum pyrolysis	450 °C	47.40 ± 2.19	65.06 ± 1.67	75.32 ± 1.24	78.12 ± 1.41
	550 °C	52.16 ± 1.12	62.49 ± 1.55	84.52 ± 1.28	84.50 ± 0.73
	650 °C	71.21 ± 1.75	78.34 ± 1.48	83.48 ± 1.89	97.90 ± 0.98

untreated samples with the treated ones. Both the untreated samples (7a) and the samples subjected to incineration (7b) appear to be composed of particles of an irregular shape with dimension <2μ. They are grouped in disorganized clusters or organized globular particles. So, the morphology has not been affected by the incineration. The pyrolyzed samples (7c) look only slightly affected, with smaller globular particles. The vacuum pyrolysis, (7d) instead, causes a significative decrease in the number of globular particles and the samples look composed only by irregular-shaped particles without any kind of grouping scheme and

with smaller size comparing with the other samples. The increasing of time of treatment (Fig. 8) does not have evident effects in the morphology except that for the samples subjected to vacuum pyrolysis (8e-f), for which the dimension of the irregular-shape particles is sensibly reduced.
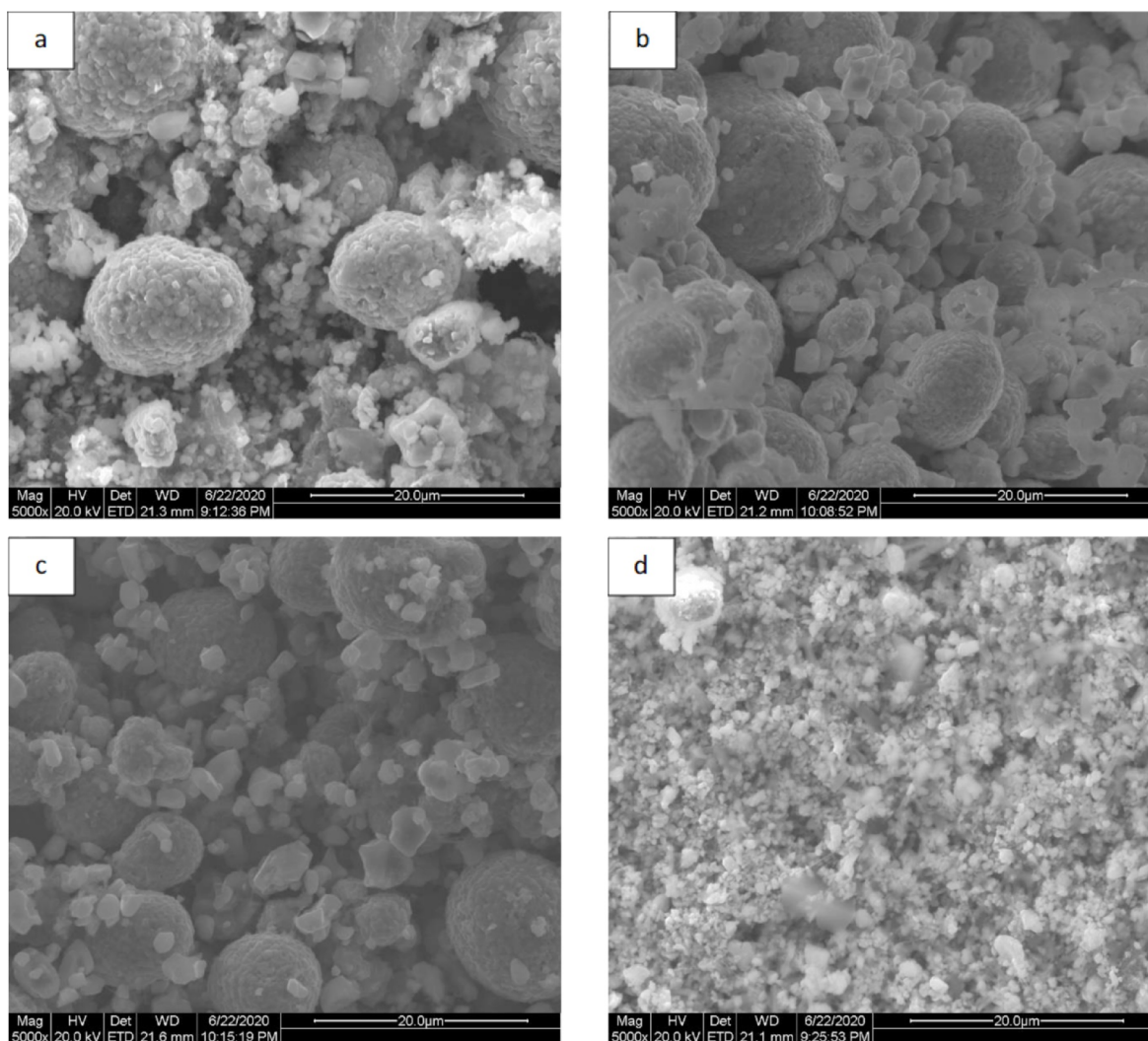

Fig. 7. SEM images of cathode active material separated from a)untreated sample, b)incinerated sample at 550C for 150 min, c) pyrolyzed under inert gas sample at 550C for 150 min, d) pyrolyzed under vacuum sample at 550C for 150 min.
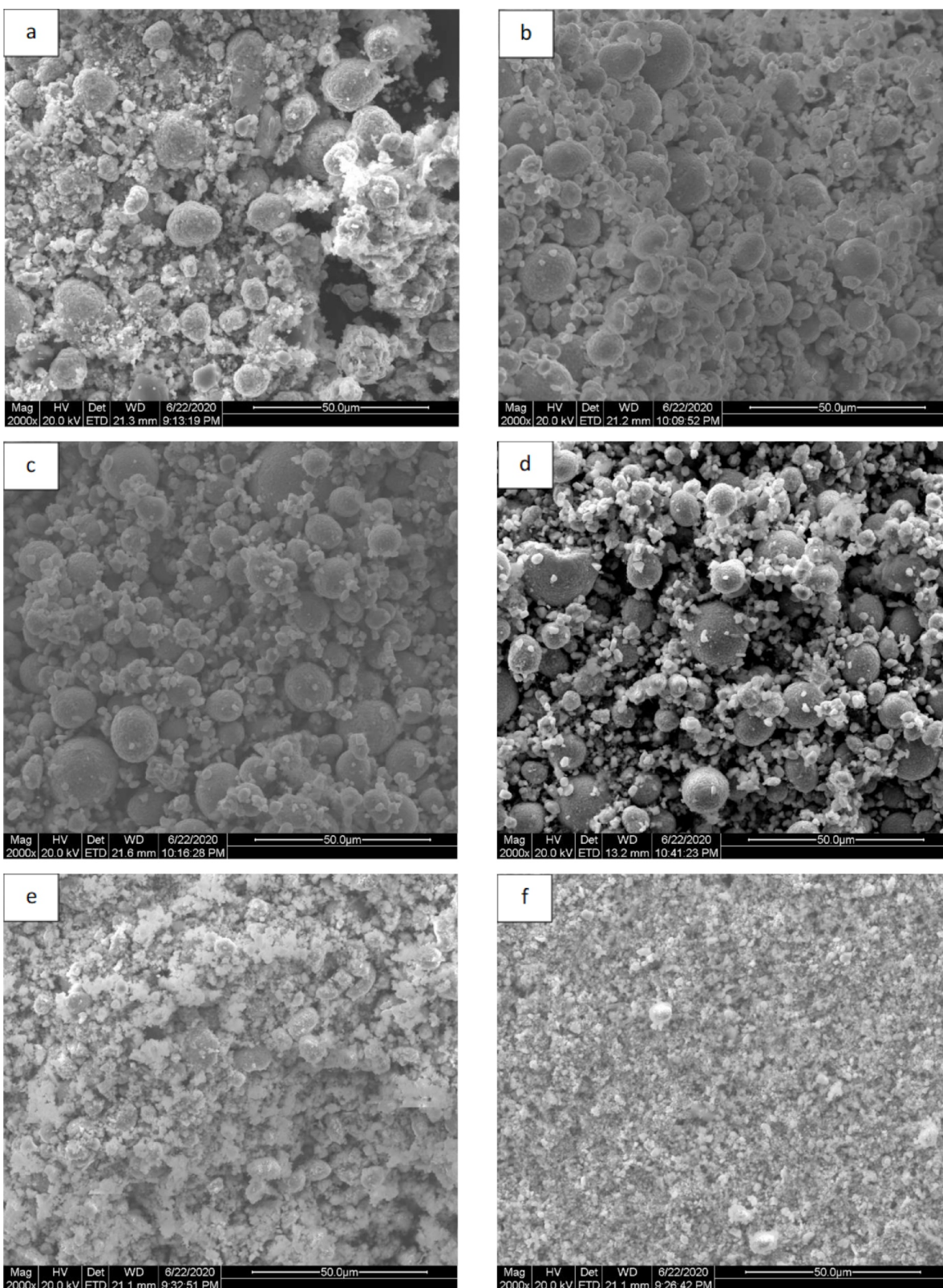
Fig. 8. SEM images of cathode active material separated from a) incinerated sample at 550C for 30 min, b)incinerated sample at 550C for 90 min, c) pyrolyzed under inert gas sample at 550C for 30 min, d) pyrolyzed under inert gas sample at 550C for 90 min, e) pyrolyzed under vacuum sample at 550C for 30 min, f) pyrolyzed under vacuum sample at 550C for 90 min.

4.8. Presence of aluminum in the cathode active material recovered after milling

Thermal treatment under oxygen determines the formation of a layer of A_2O_3 on the surface of the Al foil. This leads to an increased in the brittleness of the Al foil and could lead to increased contamination of Al powder in the removed cathode active material, which ultimately decreases the metal yield in the aluminum recycling process. In Table 3,

Table 3
Al content in the cathode active material recovered after milling (w%). Accuracy is < ± 0.15%.

		Untreated	5.15			
	Treatment time	30 min	60 min	90 min	150 min
Incineration	450 °C	0.5	0.56	1.01	1.33
	550 °C	0.91	2.04	2.95	3.16
	650 °C	1.25	2.34	3.45	4.62
Dynamic pyrolysis	450 °C	4.1	3.79	3.08	2.14
	550 °C	3.47	1.69	1.45	1.1
	650 °C	2.61	1.39	1.28	0.95
Vacuum pyrolysis	450 °C	0.8	0.81	0.67	0.57
	550 °C	0.63	0.59	0.34	0.3
	650 °C	0.45	0.36	0.23	0.23

it is possible to observe the Al content in the cathode active material recovered after milling. The content of Al increased with the time and temperature of treatment in the incinerated samples, reaching the 4.62 w% after incineration at 650 °C for 150 min. However, the higher concentration of Al was detected in the untreated removed cathode material, 5.15 w%. Furthermore, in the active material removed from the samples subjected to dynamic and vacuum pyrolysis, the concentration of Al decrease with the increasing of the time and temperature of treatment, opposite of what happens in the incinerated samples. This trend is probably due to the strong cohesion between the active material and the Al foil due, also to the presence of the PVDF. In the samples untreated, the adhesion is so strong that, when the ball mill is used to separate the active material from the metallic foil, Al powder remains attached to the separated active material. The increase of temperature and time of treatment determines the decomposition of the PVDF and the reduction of the adhesion.

5. Conclusions

In the work described in this paper, the effects of incineration, dynamic pyrolysis or vacuum pyrolysis on the composition of NMC-LiB were studied.

An increase in temperature, from 450 to 650 °C, and time, from 30 to 150 min, of treatment promotes the carbothermic reduction and the removal of the organic components and carbon. In inert or vacuum conditions Co, Ni, and Mn in the cathode materials are reduced to a lower oxidation state. Co_3O_4, NiO, and Mn_3O_4 are the main products. Li stays in the oxidation state $+1$ and forms Li_2O and Li_2CO_3. However, there is incomplete decomposition of the cathode active material and such reduction inhibits further re-utilization of cathode materials in battery production.

No changes in the composition of the samples were detected after incineration. This is due to the presence of oxygen in the system, which consumes the organic compounds and forms CO and CO_2. These results could indicate that this cathode material can be re-utilised in the production of new cathodes, but further analysis are needed.

Thermal treatment followed by milling permits the separation of the active material from the metal foils. This is due to the decomposition of the PVDF binder at high temperature. The best result, >95% of active material removed, was obtained subjecting the samples to incineration at a temperature between 550° C and 650° C for at least 90 min. For the pyrolysis, the same separation percentage was achieved by treating samples at a temperature higher than 550° C for at least 150 min. However, the increase of the temperature and time of treatment causes also the rise in the contamination of Al powder in the separated cathode active material, which decreases the metal yield in the Al recycling process.

Only the vacuum pyrolysis has relevant effects on the morphology.

In the gas by-products CO, CO_2, and HF were determined. Incineration proved to give greater environmental impact than dynamic pyrolysis due to its greater production of CO and CO_2. Incineration and dynamic pyrolysis produce very similar amounts of fluorides. By contrast, during vacuum pyrolysis, the gasses remain trapped in the furnace and the atmosphere becomes rich in CO, CO_2, hydrofluoric acid, and organic compounds that are volatile at high temperature. The latter recondense when the furnace returns to room temperature, thus preventing them from escaping as gas from the system, reducing the danger of the gas produced during the thermal process and therefore the costs of reducing the toxic substances contained therein. Another aspect that needs to be considered is the energy consumption. Vacuum pyrolysis has the advantage of not needing continuous pumping of gas into the system. But, if the goal is to obtain a carbothermal reduction of the active material, higher temperatures and longer treatment times are required for vacuum pyrolysis, as compared to dynamic pyrolysis. If, on the other hand, the goal is to obtain efficient separation of the active material and the aluminum foil, the least expensive energy treatment is incineration. This has proven capable of decomposing the PVDF over shorter times and at lower temperatures than pyrolysis.

CRediT authorship contribution statement

Gabriele Lombardo: Data curation, Formal analysis, Writing - original draft, Conceptualization, Methodology, Writing - review & editing. **Burçak Ebin:** Conceptualization, Methodology, Writing - review & editing, Supervision. **Britt-Marie Steenari:** Conceptualization, Methodology, Writing - review & editing, Supervision. **Mahmood Alemrajabi:** Conceptualization, Methodology, Writing - review & editing. **Ingrid Karlsson:** Conceptualization, Methodology, Writing - review & editing. **Martina Petranikova:** Conceptualization, Methodology, Writing - review & editing, Supervision.

Declaration of Competing Interest

The authors declare that they have no known competing financial interests or personal relationships that could have appeared to influence the work reported in this paper.

Acknowledgements

References

JCPDS – International Center for Diffraction Data, PDF – 4+, (2013), 12 Campus Blvd., Newton Square, PA 19073 – 3273 U.S.A., n.d. https://doi.org/10.11113/jt.v56.60.

Azevedo, M., Campagnol, N., Hagenbruch, T., Hoffman, K., Lala, A., Ramsbottom, O., 2018. Lithium and cobalt - a tale of two commodities. McKinsey Co. Met. Min.

Baldé, Forti, Gray, Kuehr, Stegmann, 2017. The Global E-waste Monitor 2017 - Executive Summary.

Chagnes, A., 2015. Lithium Battery Technologies, Lithium Process Chemistry. Elsevier Inc. https://doi.org/10.1016/b978-0-12-801417-2.00005-0.

Choi, S.S., Kim, Y.K., 2012. Microstructural analysis of poly(vinylidene fluoride) using benzene derivative pyrolysis products. J. Anal. Appl. Pyrolysis 96, 16–23. https://doi.org/10.1016/j.jaap.2012.02.014.

Dargaville, T.R., Celina, M.C., Elliott, J.M., Chaplya, P.M., Jones, G.D., Mowery, D.M., Assink, R.A., Clough, R.L., Martin, J.W., n.d. SANDIA REPORT Characterization, Performance and Optimization of PVDF as a Piezoelectric Film for Advanced Space Mirror Concepts.

Diaz, F., Wang, Y., Weyhe, R., Friedrich, B., 2019. Gas generation measurement and evaluation during mechanical processing and thermal treatment of spent Li-ion batteries. Waste Manag 84, 102–111. https://doi.org/10.1016/j.wasman.2018.11.029.

Diekmann, J., Hanisch, C., Loellhoeffel, T., Schälicke, G., Kwade, A., 2016. Ecologically friendly recycling of lithium-ion batteries - The lithorec-process. ECS Trans 73, 1–9. https://doi.org/10.1149/07301.0001ecst.

Ekberg, C., Petranikova, M., 2015. Lithium Batteries Recycling, in: Lithium Process Chemistry. Elsevier, pp. 233–267. https://doi.org/10.1016/B978-0-12-801417-2.00007-4.

Gaines, L., 2014. The future of automotive lithium-ion battery recycling: charting a

sustainable course. Sustain. Mater. Technol. 1–2, 2–7. https://doi.org/10.1016/j.susmat.2014.10.001.

Granata, G., Moscardini, E., Pagnanelli, F., Trabucco, F., Toro, L., 2012. Product recovery from Li-ion battery wastes coming from an industrial pre-treatment plant: lab scale tests and process simulations. J. Power Sources 206, 393–401. https://doi.org/10.1016/j.jpowsour.2012.01.115.

Hanisch, Christian, Diekmann, J., Stieger, A., Haselrieder, W., Kwade, A., 2015. Recycling of Lithium-Ion Batteries, in: Handbook of Clean Energy Systems. John Wiley & Sons, Ltd, Chichester, UK, pp. 1–24. https://doi.org/10.1002/9781118991978.hces221.

He, L.P., Sun, S.Y., Mu, Y.Y., Song, X.F., Yu, J.G., 2017. Recovery of Lithium, Nickel, Cobalt, and Manganese from Spent Lithium-Ion Batteries Using l -Tartaric Acid as a Leachant. ACS Sustain. Chem. Eng. 5, 714–721. https://doi.org/10.1021/acssuschemeng.6b02056.

Hirschler, M.M., 1982. Effect of oxygen on the thermal decomposition of poly(vinylidene fluoride). Eur. Polym. J. 18, 463–467. https://doi.org/10.1016/0014-3057(82)90184-7.

Hu, J., Zhang, J., Li, H., Chen, Y., Wang, C., 2017. A promising approach for the recovery of high value-added metals from spent lithium-ion batteries. J. Power Sources 351, 192–199. https://doi.org/10.1016/j.jpowsour.2017.03.093.

Inderherbergh, J., 1991. Polyvinylidene Fluoride (PVDF) Appearance. General Properties and Processing. Ferroelectrics 115, 295–302. https://doi.org/10.1080/00150193.1991.11876614.

International Energy Agency, 2018. Global EV Outlook 2018: towards cross-modal electrification. Global EV Outlook 2018. https://doi.org/10.1787/9789264302365-en.

Kim, D.S., Sohn, J.S., Lee, C.K., Lee, J.H., Han, K.S., Lee, Y.Il, 2004. Simultaneous separation and renovation of lithium cobalt oxide from the cathode of spent lithium ion rechargeable batteries. J. Power Sources 132, 145–149. https://doi.org/10.1016/j.jpowsour.2003.09.046.

Korthauer, R., 2018. Lithium-ion batteries: basics and applications. Lithium-Ion Batteries: Basics and Applications. https://doi.org/10.1007/978-3-662-53071-9.

Kwade, A., Haselrieder, W., Leithoff, R., Modlinger, A., Dietrich, F., Droeder, K., 2018. Current status and challenges for automotive battery production technologies. Nat. Energy 3, 290–300. https://doi.org/10.1038/s41560-018-0130-3.

Li, J., Shi, P., Wang, Z., Chen, Y., Chang, C.C., 2009. A combined recovery process of metals in spent lithium-ion batteries. Chemosphere 77, 1132–1136. https://doi.org/10.1016/j.chemosphere.2009.08.040.

Li, J., Wang, G., Xu, Z., 2016. Environmentally-friendly oxygen-free roasting/wet magnetic separation technology for in situ recycling cobalt, lithium carbonate and graphite from spent LiCoO 2 /graphite lithium batteries. J. Hazard. Mater. 302, 97–104. https://doi.org/10.1016/j.jhazmat.2015.09.050.

Li, L., Dunn, J.B., Zhang, X.X., Gaines, L., Chen, R.J., Wu, F., Amine, K., 2013. Recovery of metals from spent lithium-ion batteries with organic acids as leaching reagents and environmental assessment. J. Power Sources 233, 180–189. https://doi.org/10.1016/j.jpowsour.2012.12.089.

Lombardo, G., Ebin, B., Mark, M.R., Steenari, B.M., Petranikova, M., 2020. Incineration of EV Lithium-ion batteries as a pretreatment for recycling – Determination of the potential formation of hazardous by-products and effects on metal compounds. J. Hazard. Mater. 393, 122372. https://doi.org/10.1016/j.jhazmat.2020.122372.

Lombardo, G., Ebin, B., St Foreman, M.R.J., Steenari, B.-.M., Petranikova, M., 2019a. Chemical Transformations in Li-Ion Battery Electrode Materials by Carbothermic Reduction. ACS Sustain. Chem. Eng. 7. https://doi.org/10.1021/acssuschemeng.8b06540.

Lv, W., Wang, Z., Cao, H., Sun, Y., Zhang, Y., Sun, Z., 2018. A Critical Review and Analysis on the Recycling of Spent Lithium-Ion Batteries. ACS Sustain. Chem. Eng. 6, 1504–1521. https://doi.org/10.1021/acssuschemeng.7b03811.

Nguyen, T., 1985. Degradation of Polyfvinyl Fluoride) and Poiyfvinylidene Fluoride). J. Macromol. Sci. Part C 25, 227–275. https://doi.org/10.1080/15583728509412823.

Paulino, J.F., Busnardo, N.G., Afonso, J.C., 2008. Recovery of valuable elements from spent Li-batteries. J. Hazard. Mater. 150, 843–849. https://doi.org/10.1016/j.jhazmat.2007.10.048.

Petrániková, M., Miškufová, A., Havlík, T., Forsén, O., Pehkonen, A., 2011. Cobalt recovery from spent portable lithium accumulators after thermal treatment. Acta Metallurgica Slovaca.

Schmuch, R., Wagner, R., Hörpel, G., Placke, T., Winter, M., 2018. Performance and cost of materials for lithium-based rechargeable automotive batteries. Nat. Energy 3, 267–278. https://doi.org/10.1038/s41560-018-0107-2.

Song, D., Wang, X., Zhou, E., Hou, P., Guo, F., Zhang, L., 2013. Recovery and heat treatment of the Li(Ni1/3Co 1/3Mn1/3)O2 cathode scrap material for lithium ion battery. J. Power Sources 232, 348–352. https://doi.org/10.1016/j.jpowsour.2012.10.072.

Song, W., Liu, J., You, L., Wang, S., Zhou, Q., Gao, Y., Yin, R., Xu, W., Guo, Z., 2019. *Re*-synthesis of nano-structured LiFePO4/graphene composite derived from spent lithium-ion battery for booming electric vehicle application. J. Power Sources 419, 192–202. https://doi.org/10.1016/j.jpowsour.2019.02.065.

Bunsen, Till, Cazzola, P., D'Amore, L., Gorner, M., Scheffer, S., Schuitmaker, R., Signollet, H., Tattini, J., Paoli, J.T.L., 2019. Global EV Outlook 2019 to electric mobility. OECD iea.org 232.

UNFCCC, 2015. "Adoption of the Paris Agreement. United Nations Framework Convention on Climate Change. Paris.

Velázquez-Martínez, O., Valio, J., Santasalo-Aarnio, A., Reuter, M., Serna-Guerrero, R., 2019. A critical review of lithium-ion battery recycling processes from a circular economy perspective. Batteries 5, 5–7. https://doi.org/10.3390/batteries5040068.

Vezzini, A., 2014. Manufacturers, Materials and Recycling Technologies. Lithium-Ion Batteries: Advances and Applications. Elsevier B.V., pp. 529–551. https://doi.org/10.1016/B978-0-444-59513-3.00023-6.

Xiao, J., Li, J., Xu, Z., 2019. Challenges to Future Development of Spent Lithium Ion Batteries Recovery from Environmental and Technological Perspectives. Environ. Sci. Technol. https://doi.org/10.1021/acs.est.9b03725.

Xiao, J., Li, J., Xu, Z., 2017a. Recycling metals from lithium ion battery by mechanical separation and vacuum metallurgy. J. Hazard. Mater. 338, 124–131. https://doi.org/10.1016/j.jhazmat.2017.05.024.

Xiao, J., Li, J., Xu, Z., 2017b. Novel Approach for in Situ Recovery of Lithium Carbonate from Spent Lithium Ion Batteries Using Vacuum Metallurgy. Environ. Sci. Technol. 51, 11960–11966. https://doi.org/10.1021/acs.est.7b02561.

Xu, B., Qian, D., Wang, Z., Meng, Y.S., 2012. Recent progress in cathode materials research for advanced lithium ion batteries. Mater. Sci. Eng. R Reports 73, 51–65. https://doi.org/10.1016/j.mser.2012.05.003.

Yao, L., Feng, Y., Xi, G., 2015. A new method for the synthesis of LiNi1/3Co1/3Mn1/3O2 from waste lithium ion batteries. RSC Adv 5, 44107–44114. https://doi.org/10.1039/c4ra16390g.

Yao, Y., Zhu, M., Zhao, Z., Tong, B., Fan, Y., Hua, Z., 2018. Hydrometallurgical Processes for Recycling Spent Lithium-Ion Batteries: a Critical Review. ACS Sustain. Chem. Eng. https://doi.org/10.1021/acssuschemeng.8b03545.

Zeng, X., Li, J., 2014. Innovative application of ionic liquid to separate Al and cathode materials from spent high-power lithium-ion batteries. J. Hazard. Mater. 271, 50–56. https://doi.org/10.1016/j.jhazmat.2014.02.001.

Zhang, J., Hu, J., Zhang, W., Chen, Y., Wang, C., 2018a. Efficient and economical recovery of lithium, cobalt, nickel, manganese from cathode scrap of spent lithium-ion batteries. J. Clean. Prod. 204, 437–446. https://doi.org/10.1016/j.jclepro.2018.09.033.

Zhang, X., Xue, Q., Li, L., Fan, E., Wu, F., Chen, R., 2016. Sustainable Recycling and Regeneration of Cathode Scraps from Industrial Production of Lithium-Ion Batteries. ACS Sustain. Chem. Eng. 4, 7041–7049. https://doi.org/10.1021/acssuschemeng.6b01948.

Zheng, Y., Wang, S., Gao, Y., Yang, T., Zhou, Q., Song, W., Zeng, C., Wu, H., Feng, C., Liu, J., 2019. Lithium Nickel Cobalt Manganese Oxide Recovery via Spray Pyrolysis Directly from the Leachate of Spent Cathode Scraps. ACS Appl. Energy Mater. 2, 6952–6959. https://doi.org/10.1021/acsaem.9b01647.

Zulfiqar, S., Zulfiqar, M., Rizvi, M., Munir, A., McNeill, I.C., 1994. Study of the thermal degradation of polychlorotrifluoroethylene, poly(vinylidene fluoride) and copolymers of chlorotrifluoroethylene and vinylidene fluoride. Polym. Degrad. Stab. 43, 423–430. https://doi.org/10.1016/0141-3910(94)90015-9.